Pinball scattering

B. ECKHARDT, G. RUSSBERG

Fachbereich Physik der Philipps-Universität,
Renthof 6, D-3550 Marburg

P. CVITANOVIĆ, P. E. ROSENQVIST

Niels Bohr Institutet, Blegdamsvej 17, DK-2100 København Ø

P. SCHERER

Institut für Vegetative Physiologie der Universität Köln,
Robert Koch Str. 39, D-5000 Köln 41

Abstract

Classical and semiclassical periodic orbit expansions are applied to the dynamics of a point particle scattering elastically off several disks in a plane. Fredholm determinants, zeta functions, and convergence of their cycle expansions are tested and applied to evaluation of classical escape rates and quantum resonances. The results demonstrate the applicability of the Ruelle and Gutzwiller type periodic orbit expressions for chaotic systems.

1 Introduction

At the heart of semiclassical descriptions of chaotic systems is the Gutzwiller trace formula which relates the eigenvalue spectrum of the Schrödinger operator to the periodic orbits of the underlying classical system [1]. This relationship between the classical and the quantum properties can be viewed as a generalization of the Selberg trace formula which relates the spectrum of the Laplace-Beltrami operator to geodesic motion on surfaces of constant negative curvature [2]. Whereas the Selberg trace is exact, the Gutzwiller trace, derived within a stationary phase approximation, is only approximate, valid in a suitable semiclassical limit.

In one-dimensional systems the trace formula recovers the standard WKB quantization rules, which yield easy and sometimes quite accurate estimates for the quantum eigenvalues [3]. For systems with more than one degree of freedom a classical system can exhibit chaos. The simple WKB quantization fails and evaluation of the trace formulas can become rather difficult; in fact, it is often easier to do the full quantum calculation and to obtain the periods of classical periodic orbits from the quantum data by a Fourier transform [4]. Perhaps the main difficulty inherent in the periodic orbit quantization is the fact that for chaotic systems the number of periodic orbits grows exponentially with time, and formulas such as the Gutzwiller trace formula diverge in the regime of physical

interest [5]. One aim of the present contribution will be to summarize techniques that have been developed recently to overcome such divergences [6, 7, 8].

From the vantage point of the dynamical systems theory, the trace formulas (both the exact Selberg and the semiclassical Gutzwiller trace formula) fit into a general framework of replacing phase space averages by sums over periodic orbits [9]. For classical hyperbolic systems this is possible since the invariant density can be represented by all periodic orbits, with weights related to their instability. The semiclassical periodic orbit sums differ from the classical ones only in phase factors and stability weights; such differences may be traced back to the fact that in quantum mechanics the amplitudes rather than the probabilities are added. However, it must be emphasized that for generic nonhyperbolic systems (which we shall not discuss here), with mixed phase space and marginally stable orbits, such summations are at present hard to control, and it is not clear that the periodic orbit sums should necessarily be the computational method of choice.

For hyperbolic systems, the cycle or curvature expansions of Fredholm determinants and zeta functions have proven extremely useful in evaluating eigenvalues quickly and accurately. For classical dynamics, demonstrations of the success of this method abound [7, 10]. We shall here focus on an ideal quantum system, scattering off three (or more) disks in the plane [11]. This system was investigated in a series of papers by Gaspard and Rice [12, 13], and, independently, by us. We shall present here our (mostly previously unpublished) results. We will demonstrate that for this nontrivial system cycle expansions offer an accurate test of Gutzwiller semiclassical quantization. We shall skirt some of the more technical issues; the reader can pursue them by perusing the references.

The outline of the chapter is as follows. In the next section we introduce the model and discuss the relevant aspects of its classical dynamics. The quantum results are given in section 3, and the cycle expansions are discussed in section 4. Methods for computation of periodic orbits are sketched in appendices A and B.

2 Classical pinball

The model that we shall discuss here is simple, yet physical and instructive. One can use it to illustrate and teach, in clearly physically motivated steps, almost everything one needs to know about deterministic chaos: from Smale horseshoes, Cantor sets, Lyapunov exponents, symbolic dynamics, discrete symmetries, bifurcations, pruning and diffusion, all the way to transfer operators, thermodynamic formalism, and classical and quantum zeta functions. We shall concentrate here on semiclassical calculations and tests of Gutzwiller type periodic orbit formulas.

Our classical pinball model consists of a point particle and three identical circular disks in the plane (fig. 1(a)). The point particle is scattered elastically off the disks and moves freely between collisions. The dynamics with one or two disks is simple (there is either no or one trapped trajectory), but with three or more disks there are infinitely many trapped trajectories, forming a repeller. This repeller can
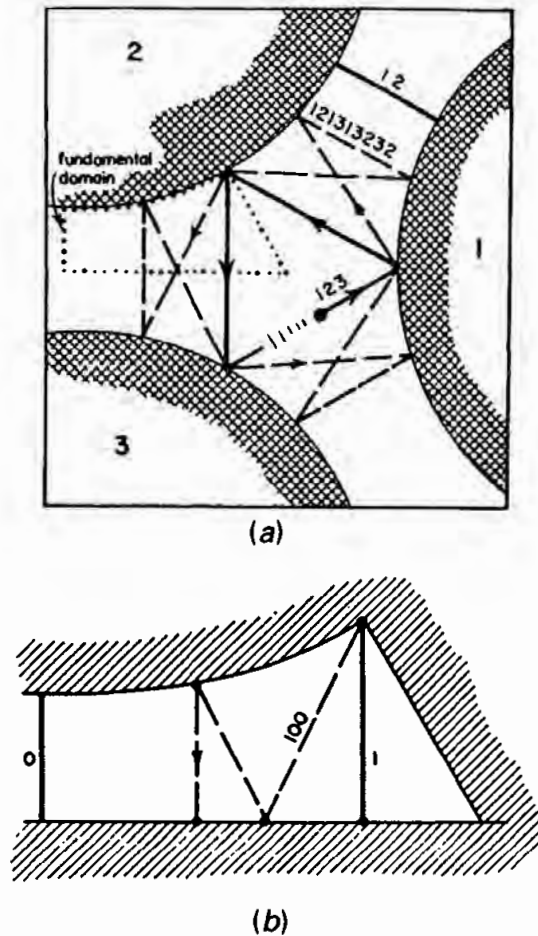
Fig. 1. The scattering geometry for the disk radius : separation ratio $R : d = 1 : 2.5$; (a) the three disks, with $\overline{12}$, $\overline{123}$ and $\overline{121232313}$ cycles indicated; (b) the fundamental domain, *i.e.*, a wedge consisting of a section of a disk, two segments of symmetry axes acting as straight mirror walls, and an escape gap. The above cycles restricted to the fundamental domain are now the two fixed points $\overline{0}$ and $\overline{1}$, and the $\overline{100}$ cycle.

be in principle observed by measurements such as irregularly fluctuating outgoing angles *vs.* impact parameter (the irregular or chaotic scattering [14]), but such measurements are difficult and very sensitive to small perturbations. Much more robust are the global averages of quantities such as the mean trapping time, which we shall discuss in what follows.

2.1 Symmetries of the model

As the three disks are equidistantly spaced, the system has C_{3v} symmetry. Applying an element (identity, rotation by $\pm 2\pi/3$, or reflection) of this symmetry group to any trajectory yields another dynamically acceptable trajectory. Symmetry operations map *nonsymmetric* orbits into different orbits of the same shape, and

for a *symmetric* orbit, the symmetry operation will map the set of points making up the orbit in phase space into itself.

For symmetric periodic orbits (a trajectory is periodic if it returns to the starting position and momentum in phase space) some or all symmetry operations act like a shift in time, advancing the starting point to the starting point of a symmetry related segment. In this way a symmetric periodic trajectory can be subdivided into a sequence of irreducible segments. Stability, action and traversal time are the same for all irreducible segments. The global periodic orbits can be described completely in terms of the irreducible segments, by folding the irreducible segments into periodic orbits in the *fundamental domain*. The fundamental domain is a one sixth slice of the full three-disk system, with the symmetry axes acting as reflecting mirrors, see fig. 1(b).

Orbits related in the full space by discrete symmetries map onto a single fundamental domain orbit. The reduction to the fundamental domain desymmetrizes the dynamics and removes all global discrete symmetry induced degeneracies: rotationally symmetric global orbits have degeneracy 2, reflectionally symmetric ones have degeneracy 3, and global orbits with no symmetry are 6-fold degenerate. The time-reversal degeneracies persist in the fundamental domain as well. Some examples of such orbits are shown in fig. 2.

2.2 Symbolic coding

The motion of a point particle is such that after a collision with one disk it either continues to another disk or it escapes to infinity. Labelling the disks 1, 2 and 3, this suggests associating with every trajectory a sequence of labels, indicating the disks with which the particle collides. The collision sequence will be finite for a scattering orbit, coming in from infinity and escaping after a finite number of collisions, and it will repeat periodically for a (trapped) periodic orbit. Arguments used in the usual horseshoe construction show that among the infinitely long sequences and the infinitely long unstable trapped orbits there is a one-to-one relationship; there exists an orbit to every (allowed) infinite sequence and every (allowed) infinite sequence labels a unique orbit.

There is one obvious restriction to the possible sequences, namely that two consecutive symbols must not be identical, since the particle cannot collide twice in succession with the same disk. In addition, there are relabelling symmetries, relating for instance the periodic orbits $\overline{12}$, $\overline{23}$, and $\overline{13}$, which are mapped into the same fundamental domain orbit. (A bar over a sequence indicates periodic repetitions; it will often be omitted when it is clear from the context that we are dealing with periodic orbits.) By replacing the absolute disk labels by relative symbols, indicating only the orientation of the motion (clockwise or anticlockwise), both the symbol repetitions and the symmetry degeneracy are removed. We shall use the symbol 1 to indicate that the orientation after collision is kept, and the symbol 0 to indicate that it is reversed. Depending
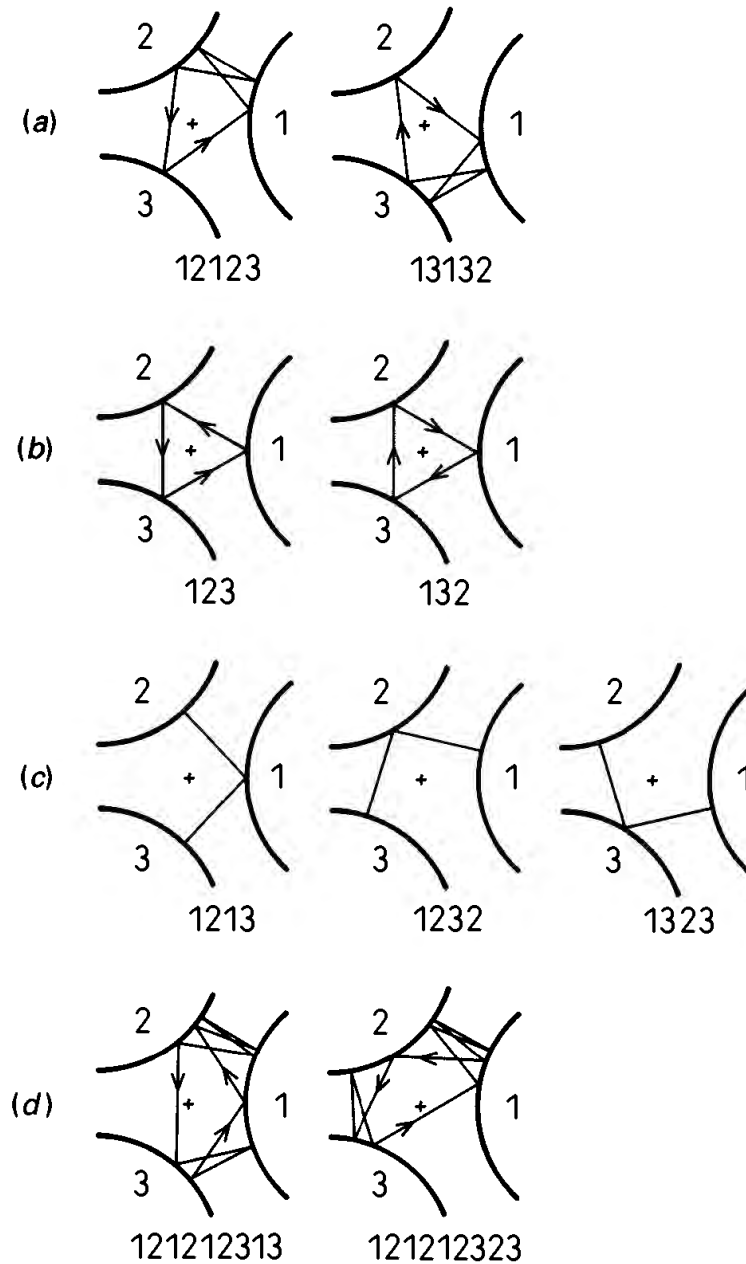
Fig. 2. Some examples of three-disk cycles: (a) $\overline{12123}$ and $\overline{13132}$ are mapped onto each other by σ_{23}, the flip across 1 axis; this cycle has degeneracy 6 under C_{3v} symmetries. Similarly (b) $\overline{123}$ and $\overline{132}$ and (c) $\overline{1213}$, $\overline{1232}$ and $\overline{1323}$ are degenerate under C_{3v}. (d) The orbits $\overline{121212313}$ and $\overline{121212323}$ are related by time reversal but not by any C_{3v} symmetry.

Table 1. C_{3v} correspondence between the binary labelled fundamental domain prime cycles $\tilde{p}$ and the full three-disk ternary $\{1,2,3\}$ cycles p, together with the C_{3v} transformation that maps the end point of the $\tilde{p}$ cycle into the irreducible segment of the p cycle. The degeneracy of p cycle is $m_p = 6n_{\tilde{p}}/n_p$.

$\tilde{p}$	p	$g_{\tilde{p}}$
0	1 2	σ_{12}
1	1 2 3	C_3
01	12 13	σ_{23}
001	121 232 313	C_3
011	121 323	σ_{13}
0001	1212 1313	σ_{23}
0011	1212 3131 2323	C_3^2
0111	1213 2123	σ_{12}
00001	12121 23232 31313	C_3
00011	12121 32323	σ_{13}
00101	12123 21213	σ_{12}
00111	12123	e
01011	12131 23212 31323	C_3
01111	12132 13123	σ_{23}
000001	121212 131313	σ_{23}
000011	121212 313131 232323	C_3^2
000101	121213	e
000111	121213 212123	σ_{12}
001011	121232 131323	σ_{23}
001101	121231 323213	σ_{13}
001111	121231 232312 313123	C_3
010111	121312 313231 232123	C_3^2
011111	121321 323123	σ_{13}

on the symmetry of the global orbit, periodically continued binary string labels correspond either to the full periodic orbit or to a repeating irreducible segment (examples are shown in fig. 1). If the disks are sufficiently far apart there are no further restrictions on symbols, and all periodic binary sequences are realized as allowed periodic orbits. Table 1 lists some of the shortest binary symbol strings, together with the corresponding full three-disk symbol sequences and orbit symmetries.

2.3 Periodic orbits

There is only one length scale in the system, the ratio of the center-to-center separation to the disk radius $d : R$. The energy is a quadratic function of

momenta, $H = p^2/2m$, so motion at different energies E and E_0 is related by the scaling $p_E \rightarrow p_0\sqrt{E/E_0}$ for momenta, $t_E \rightarrow t_0\sqrt{E_0/E}$ for times, and

$$S(E) = L\sqrt{2mE} = S(E_0)\sqrt{E/E_0} \tag{1}$$

for the actions, where L is the geometrical length of the orbit. The eigenvalues of the jacobian transverse to a periodic orbit (see below) are invariant under the above energy rescaling. These observations will be useful below in the semiclassical context where the energy in (1) will combine with $\hbar$ to the relevant quantum variable, the wave number $k = \sqrt{2mE}/\hbar$.

The motion between collisions is completely characterized by an angle s (or arclength in case of a general billiard) marking the point of collision along a disk and the impact parameter $b = b'/R = \sin\phi$ measured in units of the radius, with ϕ the incidence angle (the angle between the outgoing particle and the outgoing normal to the billiard edge). Because of symmetry, we can always select the disk 1 as the disk of current collision and disk 3 as the origin of the particle. Ingoing coordinates then are (φ_{in}, b_{in}) and outgoing coordinates are $(\tilde{\varphi}_{out}, \tilde{b}_{out})$, where the $\tilde{\ }$ indicates that these coordinates refer to the next collision disk. When working in the fundamental domain they still need to be mapped back onto disk 2. Accordingly, we have two types of collisions:

0: the particle returns to the disk it came from
1: the particle continues to the next disk.

The corresponding maps are (the angle s is measured clockwise relative to the line connecting the centers of disks 1 and 3)

$$T_0 : \begin{cases} \varphi_{out} = -\varphi_{in} + 2\arcsin b_{in} \\ b_{out} = -b_{in} + \dfrac{d}{R}\sin\varphi_{out} \end{cases} \tag{2}$$

for reflection and

$$T_1 : \begin{cases} \varphi_{out} = \varphi_{in} - 2\arcsin b_{in} + \varphi_{shift} \\ b_{out} = b_{in} - \dfrac{d}{R}\sin\varphi_{out} \end{cases} \tag{3}$$

with $\varphi_{shift} = 2\pi/3$ for the case of continuation. Each map has a fixed point, corresponding to the orbits $\bar{0}$ and $\bar{1}$. Longer periodic orbits are fixed points of sequences of maps, e.g.

$$T_0 T_0 T_1 T_0 T_1 x_{10100} = x_{10100}, \tag{4}$$

(note that in our convention the maps are applied in reverse order compared to the symbolic sequence).

The jacobian of the single collision map is given by

$$J_i = \frac{\partial T_i(\varphi_{out}, b_{out})}{\partial(\varphi_{in}, b_{in})} \tag{5}$$

and the cycle jacobian J_p is given by the product of jacobians for the bounces

around the cycle p. As the dynamics is phase-space volume preserving, $\det J = 1$, and the eigenvalues depend only on $tr(J)$:

$$\Lambda_\pm = \frac{1}{2}\left(tr(J) \pm \sqrt{tr(J)^2 - 4}\right) .\tag{6}$$

The sign of the eigenvalue depends on the number of collisions along the cycle (see appendix B). For the '0' symbol there are two bounces in the fundamental domain: one with the disk and one with the reflecting wall. Since the wall can be regarded as a disk of infinite radius, the trace changes sign twice and thus the eigenvalues are positive. Symbol '1' corresponds to one bounce with the disk but two wall bounces and hence the eigenvalues of the '1'-cycle are negative. For an arbitrary fundamental domain cycle, the eigenvalue sign is given by $(-1)^{n_1}$, where n_1 is the number of '1's in the binary string corresponding to the cycle.

The exact lengths and eigenvalues of $\overline{0}$, $\overline{1}$ and $\overline{10}$ cycles follow from elementary geometrical considerations (we set the disk radius $R = 1$ throughout). For the fundamental domain $\overline{0}$ (the 2-cycle of the complete 3-disk space) and $\overline{1}$ (the 3-cycle of the complete 3-disk space) fixed points we obtain

$$\overline{0}: \quad \varphi_0 = 0 \quad b_0 = 0 \quad L_0 = d - 2 \quad \Lambda_0 = (d-1) + \sqrt{d(d-2)}$$
$$\overline{1}: \quad \varphi_1 = 0 \quad b_1 = \frac{1}{2} \quad L_1 = d - \sqrt{3} \quad \Lambda_1 = -(\frac{2}{\sqrt{3}}d - 1) - \sqrt{\frac{2}{\sqrt{3}}d(\frac{2}{\sqrt{3}}d - 2)} ,\tag{7}$$

and for the $\overline{10}$-cycle we obtain

$$\overline{10}: \quad L_{10} = \sqrt{1 + (2d - \sqrt{3})^2} - 2,$$
$$tr(J_{10}) = \frac{L_{10}(L_{10} + 1)(L_{10} + 2)}{\sqrt{3}d/2 - 1} + 2L_{10} + 2 .\tag{8}$$

Λ_{10} follows from (6). Longer cycles require numerical evaluation by methods such as the multipoint shooting or orbit length minimization, described in the appendix A. Formulas for evaluation of the cycle jacobians are given in the appendix B. A typical set of the periodic orbit data, for $d : R = 6$ and length ≤ 6, is listed in table 2.

2.4 Classical escape rate

The interesting part of the classical scattering dynamics is generated by the chaotic repeller, formed by the trapped (periodic and aperiodic) orbits. The closure of this set in the phase space is of zero Lebesgue measure, and almost every trajectory entering the vicinity of the repeller eventually escapes. However, some will be trapped for very long times; the quantity that characterizes this phenomenon is the mean trapping time or its inverse, the *escape rate*. The escape rate can be extracted from the trace of the classical Liouville operator [15], which we interpret as follows. The probability of returning to the starting point in phase

Table 2. All periodic orbits up to six bounces for the three-disk fundamental domain at $d : R = 6$. The columns list the topological length of the cycle, its expanding eigenvalue Λ_p, the length of the orbit (for billiards this is the same as the action), and the binary code for the cycle. Note that the two period 6 orbits $\overline{001011}$ and $\overline{001101}$ are degenerate due to the time reversal symmetry, but are not related by any discrete spatial symmetry.

period	Λ_p	Action	code
1	9.898979485566	4.000000000000	0
1	$-1.177145519638 \times 10^1$	4.267949192431	1
2	$-1.240948019921 \times 10^2$	8.316529485168	01
3	$-1.240542557041 \times 10^3$	12.321746616182	001
3	$1.449545074956 \times 10^3$	12.580807741032	011
4	$-1.229570686196 \times 10^4$	16.322276474382	0001
4	$1.445997591902 \times 10^4$	16.585242906081	0011
4	$-1.707901900894 \times 10^4$	16.849071859224	0111
5	$-1.217338387051 \times 10^5$	20.322330025739	00001
5	$1.432820951544 \times 10^5$	20.585689671758	00011
5	$1.539257907420 \times 10^5$	20.638238386018	00101
5	$-1.704107155425 \times 10^5$	20.853571517227	00111
5	$-1.799019479426 \times 10^5$	20.897369388186	01011
5	$2.010247347433 \times 10^5$	21.116994322373	01111
6	$-1.205062923819 \times 10^6$	24.322335435738	000001
6	$1.418521622814 \times 10^6$	24.585734788507	000011
6	$1.525597448217 \times 10^6$	24.638760250323	000101
6	$-1.688624934257 \times 10^6$	24.854025100071	000111
6	$-1.796354939785 \times 10^6$	24.902167001066	001011
6	$-1.796354939785 \times 10^6$	24.902167001066	001101
6	$2.005733106218 \times 10^6$	25.121488488111	001111
6	$2.119615015369 \times 10^6$	25.165628236279	010111
6	$-2.366378254801 \times 10^6$	25.384945785676	011111

space after a time t is $\delta(\mathbf{x} - \mathbf{x}_t)$, so integrating over all phase space points yields the total recurrence probability

$$\sum_{p.o.} \frac{T_p}{|\det(1 - \mathbf{J}_{p.o.})|} \delta(t - T_{p.o.}),$$

where *p.o.* indicates that the sum extends over all periodic orbits, including multiple traversals; their period time (single traversal) is T_p, and the jacobian (or the monodromy matrix) of the mapping transverse to the trajectory is $\mathbf{J}_{p.o.}$. The above expression is correct if the system is hyperbolic, *i.e.*, if all periodic points are isolated and their stability eigenvalues are strictly bounded away from unity. In this case the sum decays exponentially with time, $\propto e^{-\gamma t}$, and the leading pole

of its Laplace transform

$$\Omega(s) = \sum_{p.o.} \frac{T_p}{|\det(1 - \mathbf{J}_{p.o.})|} e^{sT_{p.o.}} \tag{9}$$

yields the decay rate $s = \gamma$. Now distinguish a primitive periodic orbit p from its r-th traversal, $p.o. = rp$, and write

$$\Omega(s) = \sum_p \sum_{r=1}^{\infty} \frac{T_p}{|\det(1 - \mathbf{J}_p^r)|} e^{rsT_p} . \tag{10}$$

For a Hamiltonian two-degrees-of-freedom system, $\mathbf{J}_p$ is a $[2 \times 2]$ matrix with unit determinant. If the cycle is unstable, the eigenvalues Λ_p and $1/\Lambda_p$ are real, and we denote the expanding eigenvalue by Λ_p. The denominator can then be expanded in a geometric series

$$1/|\det(\mathbf{J}_p - 1)| = |\Lambda_p|^{-1}(1 - 1/\Lambda_p)^{-2} = |\Lambda_p|^{-1} \sum_{j=0}^{\infty} (j+1)\Lambda_p^{-j} .$$

Performing the r summation and interchanging sums and logarithms one ends up with $\Omega(s) = (\partial/\partial s) \ln F(s)$, where $F(s)$ is the classical Fredholm determinant

$$F(s) = \prod_p \prod_{j=0}^{\infty} \left(1 - |\Lambda_p|^{-1} \Lambda_p^{-j} e^{sT_p}\right)^{j+1} . \tag{11}$$

As $\Omega(s)$ is a logarithmic derivative, its poles are given by the zeros and poles of $F(s)$. Denoting the classical weight of the cycle p by

$$t_p = z^{n_p} e^{sT_p} / |\Lambda_p| \tag{12}$$

and defining dynamical zeta functions [9]

$$1/\zeta_j = \exp\left(-\sum_p \sum_{r=1}^{\infty} \frac{1}{r}(t_p/\Lambda_p^j)^r\right) = \prod_p \left(1 - t_p/\Lambda_p^j\right) , \tag{13}$$

the Fredholm determinant can be written as an infinite product over $1/\zeta_j$:

$$F(s) = \prod_p \prod_{j=0}^{\infty} (1 - t_p/\Lambda_p^j)^{j+1} = \prod_{j=0}^{\infty} 1/\zeta_j^{j+1} . \tag{14}$$

We have introduced a bookkeeping variable z raised to the power of the topological length (number of disk collisions in a cycle) in order to be able systematically to expand the infinite products in terms of increasing topological cycle length.

Postponing a discussion of both the cycle expansions and their convergence until we have introduced the corresponding quantum objects, we present the results for the classical escape rate, computed by using $1/\zeta_0$ from eq. (13), in fig. 3. For sufficiently separated disks, already period 2 cycles yield results in good agreement with the Monte Carlo simulation estimates, demonstrating that
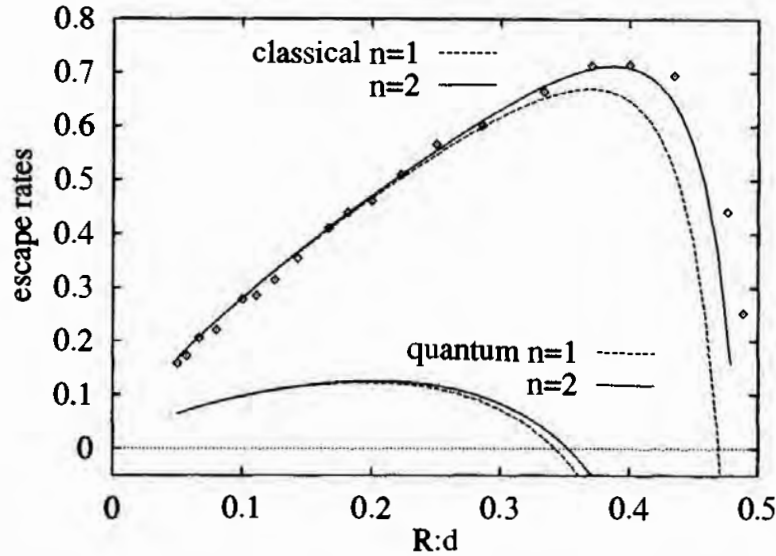
Fig. 3. Classical escape rates and bounds on quantum escape rates, *i.e.* the zeros of the zeta functions (11) and (17) with absolute weights (19), as functions of the disk-disk separation. The top two curves show the classical escape rate. Zeros computed from fixed points alone are shown as dotted lines, zeros from fixed points and period two orbits as full lines, and the Monte Carlo estimates of classical escape rates [12, 18] are marked by diamonds. The classical escape rate should approach 0 as $R : d \to 0.5$; in this limit cycle expansions are expected to converge poorly due to pruning and intermittency effects. The lower two curves show s_c, the abscissa of absolute convergence of the Gutzwiller trace formula, which serves as a crude lower bound on the imaginary part of the semiclassical quantum resonances. Though this bound becomes negative near $R : d \approx 0.33$, the semiclassical resonances do remain below the real energy axis, see fig. 4.

the zeta function formalism offers a powerful method for evaluation of escape rates.

3 Quantum pinball

For the three-disk system, the explicit expressions of the outgoing waves in terms of the ingoing waves using the quantum scattering matrix S have been given by Gaspard and Rice [13]. Resonances are related to complex zeros of $\operatorname{tr} S^{\dagger}(dS/dE)$, the generalization of the concept of the density of states to scattering systems [16]. We shall first evaluate these complex zeros in the semiclassical approximation, and then compare them with the exact quantum-mechanical resonances.

3.1 The semiclassical density of states

In the Gutzwiller's semiclassical approximation [1], the oscillatory part of the density of states is given by

$$\rho(E) = -\mathrm{Im}\frac{1}{i\pi\hbar}\sum_{p}\sum_{r=1}^{\infty}\frac{T_p}{|\det(1 - J_p^r)|^{1/2}}e^{ir(S_p/\hbar-\mu_p\pi/2)} . \tag{15}$$

For billiards the Maslov indices μ_p count the number of collisions, with a phase loss of π at every collision off a hard wall. The group-theoretic weights associated with reducing the dynamics to irreducible representations of the discrete symmetry group can sometimes also be absorbed into the phase indices. In the A_1 representation, one has only reflections at the disks, none at the boundaries of the fundamental domain. Therefore, $\mu_p = 2n_p$, since the symbol string length counts the number of the disk collisions. For the A_2 representation, the wave function is antisymmetric under reflections at the symmetry lines, and one can associate one additional reflection with each occurrence of the symbol 0, and two reflections with each occurrence of the symbol 1. The net effect is an additional overall minus sign, if the number of 0s in the symbol string of the orbit is odd. However, in general (for example, for the two-dimensional E representation of the C_{3v} discrete group) a full group-theoretic decomposition in terms of group characters is required [19]. Furthermore, special attention should be paid to the orbits that run along the borders of the fundamental domain. The three-disk system studied here does not have boundary orbits, but the four-disk system, for example, does have such orbits.

As mentioned above one can replace $S_p(E)/\hbar = L_p k$, where L_p is the geometric length of the orbit, and k is the wave number. Expressing the density as a function of k, and manipulating the denominator as in sect. 2.4, one finds

$$\rho(k) = -\mathrm{Im}\frac{1}{\pi}\frac{\partial}{\partial k}\log Z(k) \tag{16}$$

where $Z(k)$ is the *quantum Selberg zeta* function [17]

$$Z(k) = \prod_{j=0}^{\infty}\prod_{p}(1 - e^{iL_p k - i\mu_p\pi/2}|\Lambda_p|^{-1/2}\Lambda_p^{-j}). \tag{17}$$

The quantum Selberg zeta function can also be expressed as a product over dynamical zeta functions (13),

$$Z(k) = \prod_{j=0}^{\infty}1/\zeta_j , \tag{18}$$

this time with cycles weighted by semiclassical weights

$$t_p = z^{n_p}e^{iS_p/\hbar - i\mu_p\pi/2}/|\Lambda_p|^{1/2} . \tag{19}$$

We have evaluated several hundreds of semiclassical and exact quantum resonances in the three symmetry subspaces A_1, A_2 and E; some of them are listed
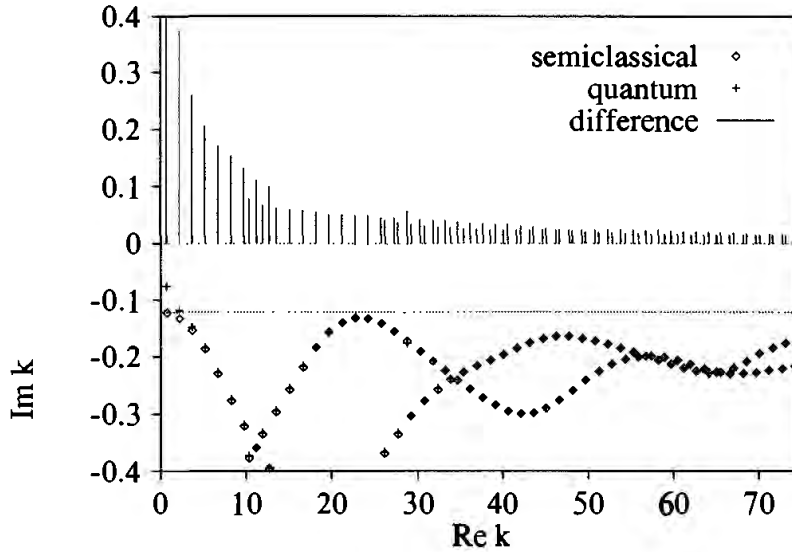
Fig. 4. Semiclassical scattering resonances (diamonds) compared with the exact quantum scattering resonances (crosses) in the A, subspace. The lines in the upper half of the diagram indicate the (geometrical) difference between the semiclassical and quantum resonances for all resonances with Im $k > -0.4$, magnified by a factor 10. The dotted line at $k_c = -0.121556$ indicates the semiclassical abscissa of convergence; all semiclassical resonances lie below this line, but the first two quantum resonances lie above it. For the semiclassical calculation, all orbits up to symbolic length 5 have been used in the cycle expansion for ζ_0^{-1}.

in table 3 and plotted in fig. 4. The accuracy and numerical convergence of the semiclassical estimates came as a surprise [8].

3.2 "Quantum escape rate"

The region of absolute convergence of the Gutzwiller trace formula in the $k = \kappa - is$ complex plane is determined by the convergence of the sum of absolute values of the terms in the series (15). The sum converges absolutely for $s < s_c$, where s_c is called the abscissa of absolute convergence. Since s_c is the value of s for which the sum

$$\tilde{\Omega}(s) = \sum_{p.o.} \frac{T_p}{|\det(1 - \mathbf{J}_{p.o.})|^{1/2}} e^{sT_{p.o.}}, \tag{20}$$

diverges, one can, by analogy with the determination of the classical escape rate by the divergence of sum (9), interpret the abscissa of absolute convergence s_c as a "quantum escape rate". In fact, s_c is only a lower bound on the escape rate; the correct rate of a decay of a given initial wave function is given by a superposition of complex resonances evaluated below. Within the same short cycles truncations as in the classical case, one finds the s_c curves shown in the lower half of fig. 3.

Table 3. Several subsets of semiclassical and quantum resonances for $d : R = 6$. The A_1 subspace resonances are plotted in Fig. 4.

	Re k_{QM}	Im k_{QM}	Re k_{zeta}	Im k_{zeta}
	0.69800	-0.07497	0.75831	-0.12282
	2.23960	-0.11880	2.27427	-0.13305
	3.76270	-0.14756	3.78787	-0.15412
	4.13165	-0.61702	4.15179	-0.66591
	5.27569	-0.18325	5.29607	-0.18678
	6.77609	-0.22750	6.79366	-0.22986
	8.26114	-0.27492	8.27663	-0.27698
	9.73452	-0.13880	9.74826	-0.32121
	10.33819	-0.37371	10.34656	-0.37834
	11.20210	-0.35823	11.21361	-0.36168
A_1	11.90760	-0.33223	11.91448	-0.33488
	12.66760	-0.39467	12.67500	-0.39841
	13.47692	-0.29412	13.48266	-0.29623
	14.13370	-0.42883	14.13680	-0.42956
	15.04170	-0.25552	15.04705	-0.25762
	16.59706	-0.21700	16.60244	-0.21889
	18.14115	-0.18280	18.14647	-0.18426
	19.67567	-0.15653	19.68084	-0.15761
	21.20308	-0.13958	21.20807	-0.14032
	22.72484	-0.13187	22.72966	-0.13235
	24.24120	-0.13284	24.24588	-0.13311
	25.75156	-0.14130	25.75605	-0.14153
	7.93363	-0.15129	7.94561	-0.15526
	9.45604	-0.13196	9.46661	-0.13458
	10.97616	-0.12325	10.98563	-0.12504
	12.49347	-0.12432	12.50215	-0.12550
	14.00693	-0.13468	14.01501	-0.13534
	15.51469	-0.15329	15.52229	-0.15368
A_2	17.01453	-0.17810	17.02178	-0.17836
	18.50574	-0.20544	18.51273	-0.20573
	19.99011	-0.23236	19.99681	-0.23275
	20.54565	-0.31325	20.54989	-0.31495
	21.46993	-0.25775	21.47596	-0.25817
	22.10098	-0.28557	22.95261	-0.28199
	22.94703	-0.28164	23.66203	-0.26365
	18.85038	-0.17271	18.56037	-0.17350
	19.44833	-0.25471	19.45385	-0.25454
E	20.37203	-0.17461	20.37745	-0.17502
	20.94214	-0.28849	20.94718	-0.28767
	21.88904	-0.19045	21.89438	-0.19059

Since the trace formulas are convergent in the domain of absolute convergence, one cannot have zeros of the zeta function or resonances of the S-matrix in that domain. In particular, for sufficiently large $d : R$, all resonances will stay a finite distance from the real axis. In contrast to the classical case, for $d : R$ less than about 2.8 the bound s_c actually becomes negative. As we shall see below, the semiclassical resonances do lie below the real axis, as they should; but this serves as a reminder that the resonances (and the energy eigenvalues for bound systems) are being evaluated in a region where cycle expansions are only conditionally convergent, and one has to be very careful in ordering terms in such expansions.

The same absolute convergence arguments can be applied to the dynamical zeta functions. Their logarithmic derivatives correspond to sums over orbits of form

$$-\frac{\partial}{\partial k}\ln\zeta_j = i\sum_p L_p \frac{e^{iL_p k - i\mu_p \pi/2}}{|\Lambda_p|^{1/2}\Lambda_p^j}. \tag{21}$$

Due to the extra powers of Λ_p's present in $1/\zeta_j$ cycle weights, the corresponding abscissas of absolute convergence form an ordered sequence $s_j < s_{j-1} < \cdots < s_0$. The resonances closest to the real axis - which will be noticable as the sharpest resonances - should be due to zeros in $1/\zeta_0$ since the leading zeros of other $1/\zeta_j$ have larger imaginary parts. We often find it convenient to use this fact and restrict our numerical work to the leading zeros of $1/\zeta_0$ rather than the full Selberg zeta functions.

3.3 Quantum resonances

We evaluate the exact quantum mechanical resonances by the method described by Gaspard and Rice [13], which we have improved by implementing a symmetry reduced code. A comparison of resonances obtained from cycle expansions truncated to the 14 cycles of periods ≤ 5 with the exact quantum values is given in table 3 and in fig. 4, together with the difference between the semiclassical and quantum resonances $\delta = \sqrt{|k_{QM} - k_{sc}|}$. Numerically this difference seems to decrease with increasing Re k, i.e., with approach to the semiclassical limit. As the semiclassical approximation ignores terms of higher order in $\hbar$, one expects on general grounds this difference to approach a nonzero constant. Our data are insufficient to estimate the asymptotic behaviour and to bound it away from zero.

Also shown in fig. 4 is the abscissa of absolute convergence s_c. No semiclassical resonance lies above it. Two of the lowest exact quantum resonances, for which the semiclassical approximation error is largest, do lie above s_c, but that is acceptable as the bound is semiclassical.

4 Cycle expansions

The periodic orbit formulas for classical and semiclassical escape rates and reso-
nances introduced above are in practice evaluated by expanding the appropriate
zeta functions and determinants as *cycle expansions*:

$$F(z) = \sum_{j=0}^{N_{max}} C_j z^j , \qquad (22)$$

and investigating their zeros and radii of convergence as functions of truncations
to finite numbers of shortest cycles. The bookkeeping variable z that keeps
track of the topological cycle length n_p is set to $z = 1$ in actual calculations.
The evaluation of cycle expansions is facilitated by understanding the analytic
properties of $F(z)$, by judicious use of the symmetries of classical dynamics, and
by topology guided rearrangements of terms in the expansions. As we shall see
below, the main virtue of cycle expansions is their fast convergence.

4.1 Symmetry factorizations

Discrete symmetries of the classical dynamics play a role with which we are famil-
iar from quantum mechanics; as they commute with the evolution operators, they
can be used to decompose them and factorize the associated determinants [19]:

$$1/\zeta^{3-disk} = \prod_\alpha 1/\zeta_\alpha^{d_\alpha} .$$

The product is over the d_α-dimensional irreducible representations α of the
symmetry group, in this case C_{3v}, with two one-dimensional representations A_1,
A_2 and a pair of two-dimensional representations E. The factorization relates
each fundamental domain orbit to the corresponding degenerate set of full space
orbits as follows:

symmetry	full space		A_1	A_2	E
rotation	$(1 - t_{rot}^3)^2$	$=$	$(1 - t_{rot})$	$(1 - t_{rot})$	$(1 + t_{rot} + t_{rot}^2)^2$
reflection	$(1 - t_{ref}^2)^3$	$=$	$(1 - t_{ref})$	$(1 + t_{ref})$	$(1 - t_{ref}^2)^2$
none	$(1 - t_{non})^6$	$=$	$(1 - t_{non})$	$(1 - t_{non})$	$(1 - t_{non})^4$

Fundamental domain cycles up to length 5 are listed in table 1, together
with the symmetry factors that map them into the corresponding global orbit
irreducible segments; these determine which of the above factorizations apply to
a given cycle. Substituting the shortest cycles into the zeta functions, we obtain
for the completely symmetric A_1 subspace:

$$
\begin{aligned}
1/\zeta_{A_1}(z) = \ & (1 - zt_0)(1 - zt_1)(1 - z^2 t_{01})(1 - z^3 t_{001})(1 - z^3 t_{011}) \\
& (1 - z^4 t_{0001})(1 - z^4 t_{0011})(1 - z^4 t_{0111})(1 - z^5 t_{00001})(1 - z^5 t_{00011}) \\
& (1 - z^5 t_{00101})(1 - z^5 t_{00111})(1 - z^5 t_{01011})(1 - z^5 t_{01111}) \dots . \qquad (23)
\end{aligned}
$$

In the example at hand, with complete symbolic dynamics and no pruning rules, the cycle expanded zeta function is obtained by expanding the infinite product as a power series in z:

$$
\begin{aligned}
1/\zeta_{A_1}(z) \;=\; & 1 - zt_0 - zt_1 - z^2[(t_{01} - t_1 t_0)] \\
& -z^3[(t_{001} - t_{01}t_0) + (t_{011} - t_{01}t_1)] \\
& -z^4[(t_{0001} - t_0 t_{001}) + (t_{0111} - t_{011}t_1) \\
& +(t_{0011} - t_{001}t_1 - t_0 t_{011} + t_0 t_{01}t_1)] - \dots .
\end{aligned}
\tag{24}
$$

For the A_2 subspace cycles with an odd number of 0s pick up an additional minus sign:

$$
\begin{aligned}
1/\zeta_{A_2}(z) \;=\; & 1 + zt_0 - zt_1 + z^2[(t_{01} - t_1 t_0)] \\
& -z^3[(t_{001} - t_{01}t_0) - (t_{011} - t_{01}t_1)] \\
& +z^4[(t_{0001} - t_0 t_{001}) + (t_{0111} - t_{011}t_1) \\
& -(t_{0011} - t_{001}t_1 - t_0 t_{011} + t_0 t_{01}t_1)] - \dots .
\end{aligned}
\tag{25}
$$

The E subspace cycle expansion takes a somewhat less obvious form [19]:

$$
\begin{aligned}
1/\zeta_E \;=\; & (1 + zt_1 + z^2 t_1^2)(1 - z^2 t_0^2)(1 + z^3 t_{100} + z^6 t_{100}^2)(1 - z^4 t_{10}^2) \\
& (1 + z^4 t_{1001} + z^8 t_{1001}^2)(1 + z^5 t_{10000} + z^{10} t_{10000}^2) \\
& (1 + z^5 t_{10101} + z^{10} t_{10101}^2)(1 - z^{10} t_{10011})^2 \dots \\
\;=\; & 1 + zt_1 + z^2(t_1^2 - t_0^2) + z^3(t_{001} - t_1 t_0^2) \\
& +z^4\left[t_{0011} + (t_{001} - t_1 t_0^2)t_1 - t_{01}^2\right] \\
& +z^5\left[t_{00001} + t_{01011} - 2t_{00111} + (t_{0011} - t_{01}^2)t_1 + (t_1^2 - t_0^2)t_{100}\right] + \dots
\end{aligned}
\tag{26}
$$

All our numerical results are obtained by determining the zeros of finite cycle length truncations of the above cycle expansions, or the corresponding ones for the Fredholm determinats and quantum Selberg zeta functions. The crucial question that we now turn to is - how good are such truncations?

5 Convergence of cycle expansions

While various periodic orbit formulas, such as the Gutzwiller trace formula and the quantum Selberg zeta function, are formally equivalent, in practice determinants have much better convergence properties than the traces. This can be understood on two levels: a geometrical one, as shadowing of long cycles by shorter ones, or more abstractly, as a consequence of analytic properties of the Fredholm determinants. Particularly strong results exist for nice, "Axiom A" hyperbolic systems, for which the dynamical zeta functions are holomorphic [9], and the Fredholm determinants are entire functions [20].
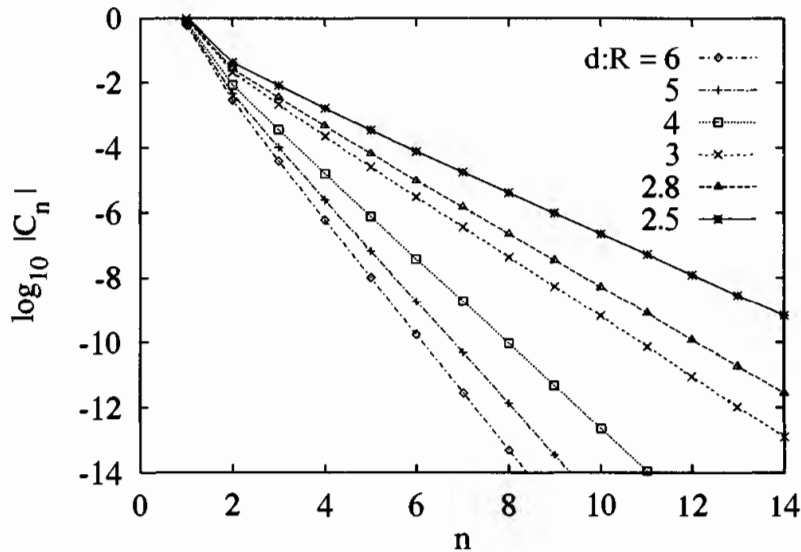
Fig. 5. The coefficients of the cycle expansion for $1/\zeta_0$ for six $d : R$ ratios (from top to bottom: $d : R = 6, 5, 4, 3, 2.8, 2.5$). Clearly visible is the exponential decay; the slope yields the location of the leading pole of $1/\zeta_0$.

5.1 Cycle shadowing and convergence

The important feature to note in the cycle expansion (24) is that the contributions t_0 and t_1 from the two fixed points stand isolated, while all others come in groups. This is seen particularly clearly if the weights are set to $t_p = 1$; in this case the zeta function reduces to the topological polynomial, *i.e.*, the generating polynomial for counting the numbers of topologically distinct cycles. For a complete binary coding without pruning rules, the topological polynomial is just $1 - 2z$, so all longer orbits appear in groups with signs and the numbers of terms such that they cancel. The success of the cycle expansion relies on the extent to which these cancellations survive when t_p are set equal to the true periodic orbit weights.

The effect of such cancellations is illustrated by fig. 5 which demonstrates that the coefficients in the cycle expansion of the dynamical zeta function $1/\zeta_0$ with quantum weights (19) fall off exponentially. The coefficients are evaluated for wave number $k = 0$ and for a range of $d : R$ ratios. Note that also for the cases $d : R = 2.5$ and 2.8, which lie outside the domain of absolute convergence (see fig. 3), there is no qualitative change in the behaviour of the coefficients.

The rate of fall-off of the cycle expansion coefficients can be estimated by observing that for subshifts of finite type [6, 7] the contributions from longer orbits can always be grouped in shadowing combinations such as $t_{a^jb} - t_a t_{a^{j-1}b}$, involving a long cycle $\overline{a^jb}$ and a pseudo-cycle built by shadowing $\overline{a^jb}$ by $\overline{a}$ followed by $\overline{a^{j-1}b}$. These orbits are periodic approximations to an orbit homoclinic to $\overline{a}$.

Table 4. Demonstration of curvature compensations in $t_{ab} - t_a t_b$ for the three disk fundamental domain cycles at $d : R = 6$, table 1.

n	$t_{ab} - t_a t_b$	$L_{ab} - (L_a + L_b)$	$\log\left[\frac{\Lambda_a\Lambda_b}{\Lambda_{ab}}\right]$	ab-a*b
2	$-5.23465150784\times10^{-4}$	$4.85802927371\times10^{-2}$	$-6.29365864467\times10^{-2}$	01-0*1
3	$-7.96028600139\times10^{-6}$	$5.21713101432\times10^{-3}$	$-9.82663364947\times10^{-3}$	001-0*01
4	$-1.03326529874\times10^{-7}$	$5.29858199419\times10^{-4}$	$-1.26966635483\times10^{-3}$	0001-0*001
5	$-1.27481522016\times10^{-9}$	$5.35513574697\times10^{-5}$	$-1.55176109954\times10^{-4}$	00001-0*0001
6	$-1.52544704823\times10^{-11}$	$5.40999882625\times10^{-6}$	$-1.83824278428\times10^{-5}$	000001-0*00001
2	$-5.23465150784\times10^{-4}$	$4.85802927371\times10^{-2}$	$-6.29365864467\times10^{-2}$	01-0*1
3	$5.30414752996\times10^{-6}$	$-3.67093656690\times10^{-3}$	$7.71831060288\times10^{-3}$	011-01*1
4	$-5.40934261680\times10^{-8}$	$3.14925761316\times10^{-4}$	$-9.23436155345\times10^{-4}$	0111-011*1
5	$4.99129508833\times10^{-10}$	$-2.67292822795\times10^{-5}$	$1.00342411247\times10^{-4}$	01111-0111*1
6	$-4.39246000586\times10^{-12}$	$2.27087116266\times10^{-6}$	$-1.03941678234\times10^{-5}$	011111-01111*1

Substituting $t_{a^j b}$ from (13) one finds

$$\frac{t_{a^j b} - t_a t_{a^{j-1} b}}{t_{a^j b}} = 1 - e^{i(S_a + S_{a^{j-1}b} - S_{a^j b})/\hbar} e^{-i\pi(\mu_a + \mu_{a^{j-1}b} - \mu_{a^j b})/2} \left|\frac{\Lambda_a\Lambda_{a^{j-1}b}}{\Lambda_{a^j b}}\right|^{-1/2}.$$

The phase factors cancel since the number and the kind of symbols involved in both terms coincide (though for the E representation of C_{3v} this is admittedly not obvious). Furthermore, since with increasing j segments of $\overline{a^j b}$ come closer to $\bar{a}$, the differences in action and the ratio of the eigenvalues converge exponentially with the eigenvalue of the orbit $\bar{a}$,

$$S_a + S_{a^{j-1}b} - S_{a^j b} \approx const \times \Lambda_a^{-j}, \quad |\Lambda_a\Lambda_{a^{j-1}b}/\Lambda_{a^j b}| \approx \exp(-const \times \Lambda_a^{-j})$$

Expanding the exponentials one thus finds that this term in the cycle expansion is of the order of

$$t_{a^j b} - t_a t_{a^{j-1}b} \approx const \times t_{a^j b}\Lambda_a^{-j}. \tag{27}$$

Even though the number of terms in a cycle expansion grows exponentially [7], the shadowing cancellations improve the convergence by an exponential factor compared to trace formulas, and extend the radius of convergence of the periodic orbit sums. Table 4 shows some examples of such compensations between long cycles and their pseudo-cycle shadows.

The shadowing cancellations require that a long cycle and the associated pseudo-cycles (products of shorter cycles following the same symbol sequence) have nearly the same weight *and* a relative minus sign. The first requirement is guaranteed by the hyperbolicity and the smoothness of the flow. The second requirement implies that, contrary to the "semi-classical" intuition, the cycle expansions are expected to converge for *low energies*. For sufficiently high wave numbers k the differences in actions $S_p - S_{shadow} = k(L_p - L_{shadow})$ can be of order
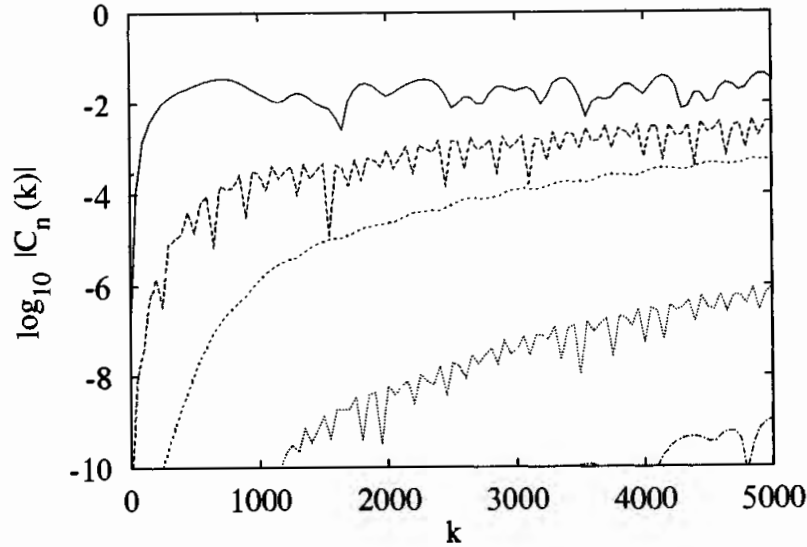
Fig. 6. Energy dependence of the cycle expansion coefficients for $d : R = 6$. Shown are (from top to bottom) the absolute values of the coefficients C_4, C_6, C_8, C_{10} and C_{12} (barely visible in the lower right corner) as a function of the wave number k.

π or higher, in which case $t_p - t_{shadow} \approx 2t_p$, rather than $t_p - t_{shadow} \approx t_p/|\Lambda_p|$ expected at $k = 0$. This is illustrated in fig. 6, which shows the energy dependence of the coefficients ($\text{Im}k = 0$) in the cycle expansion of the quantum Selberg zeta function (17). It is encouraging to note that the shadowing cancellations persist for very large intervals in k, so for the three-disk system studied here the lowest few terms in the cycle expansion suffice for evaluation of thousands of the lowest semiclassical resonaces.

5.2 Convergence of Fredholm determinants

While the above shadowing analysis of cycle expansions implies exponential convergence, cycle expansions can actually converge even faster than exponentially. If the dynamical evolution can be cast in terms of a transfer operator multiplicative along the flow, if the corresponding mapping (for example, the return map for a Poincaré section of the flow) is analytic, and if the topology of the repeller is given by a finite Markov partition, then the Fredholm determinant (14) with classical weight (12) is *entire*. This has been recently proven by H.H. Rugh [20] (earlier mathematical literature dealt only with the expanding directions, not the full hyperbolic flow). In this case the cycle expansion coefficients (22) fall off asymptotically as $C_n \approx \Lambda^{-n^{3/2}}$. This estimate is in agreement with our numerical results for the three-disk repeller, see fig. 9. However, as it is not known how quickly the asymptotics should set in, such numerical results can be misleading, and preasymptotic oscillations can already be observed in simple one-dimensional
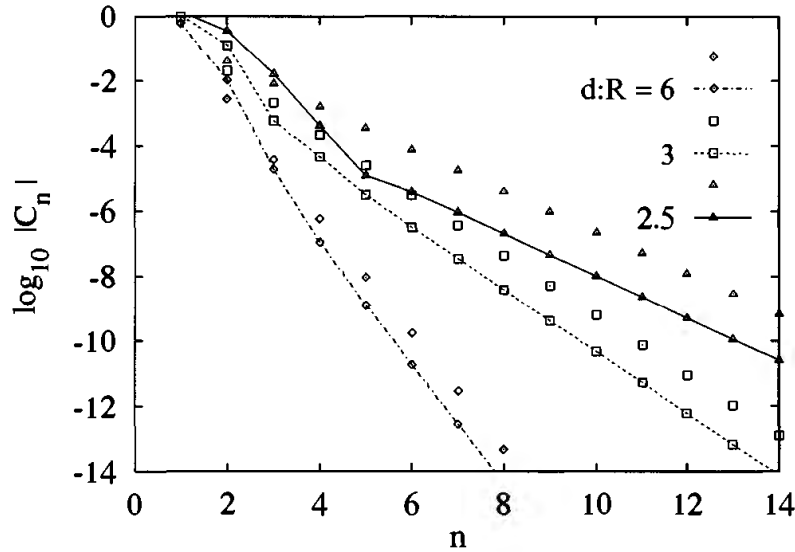
Fig. 7. The coefficients of the cycle expansion for the quantum Selberg zeta function $Z_{qm}(z)$ (connected with lines) and for $1/\zeta_0$ (not connected) for ratios $d : R = 6$ (diamonds), 3 (squares) and 2.5 (triangles). Note that the asymptotic slopes for the quantum Selberg zeta functions and the dynamical zeta functions are the same; the double pole present in the dynamical zeta function persists as a single pole in the Selberg product.

repellers. In the present case, such preasymptotic oscillations are noticable in data for larger disk-disk spacings.

5.3 Poles of dynamical zeta functions

The exponential decay of the coefficients for $1/\zeta_0$ indicates the presence of a pole. Numerical investigations [21] of both the classical and the quantum dynamical $1/\zeta_j$ functions for two-dimensional Hamiltonian flows indicate that a $1/\zeta_j$ function has a *double* pole coinciding with the leading zero of $1/\zeta_{j+1}$. Consequently $1/\zeta_0$, $1/\zeta_0\zeta_1$ and the quantum Selberg zeta function all have the same leading pole, and coefficients in their cycle expansions fall off exponentially with the same slope, fig. 7. Multiplying the quantum Selberg zeta function by $(1 - z/z_1)$, where z_1 is the leading zero of $1/\zeta_1(z)$, one obtains faster, but still exponential decay in the coefficients, indicating further poles down in the complex plane (see fig. 8).

The double pole is not as surprising as it might seem at first glance; indeed, the theorem that establishes that the classical Fredholm determinant (14) is entire implies that the poles in $1/\zeta_j$ must have right multiplicities in order that they be cancelled in the $F = \prod 1/\zeta_j$ product [22]. More explicitly, $1/\zeta_j$ can be expressed in terms of weighted Fredholm determinants

$$F_j = \exp\left(-\sum_p \sum_{r=1}^{\infty} \frac{1}{r} \frac{(t_p/\Lambda_p^j)^r}{(1 - 1/\Lambda_p^r)^2}\right) \tag{28}$$
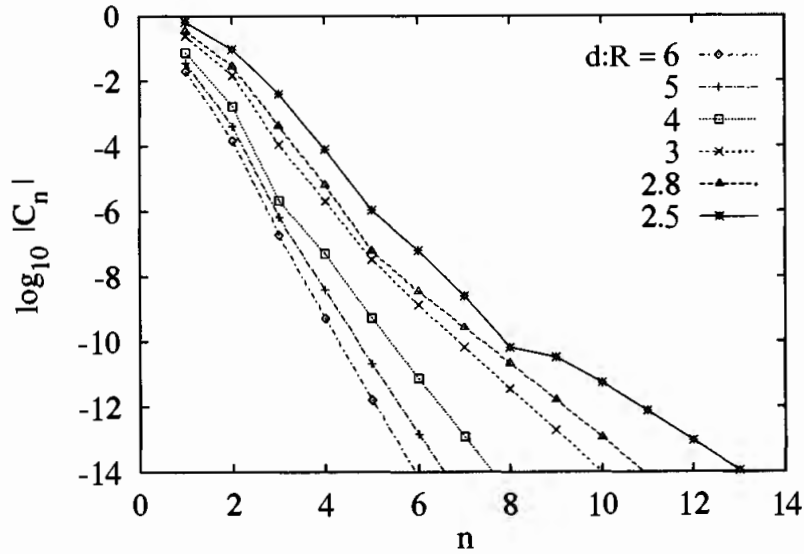
Fig. 8. The coefficients of the cycle expansion for the quantum Selberg zeta function $Z_{qm}(z)$ after multiplication with $(1 - z/z_1)$ where z_1 is the zero of $\zeta_1^{-1}(z)$. The coefficients still decay only exponentially but with much steeper slope, indicating the presence of yet another pole.

by inserting the identity

$$1 = \frac{1}{(1 - 1/\Lambda)^2} - \frac{2}{\Lambda}\frac{1}{(1 - 1/\Lambda)^2} + \frac{1}{\Lambda^2}\frac{1}{(1 - 1/\Lambda)^2}$$

into the exponential representation (13) of $1/\zeta_j$. This yields

$$1/\zeta_j = \frac{F_j F_{j+2}}{F_{j+1}^2} \, , \tag{29}$$

and we conclude that for two-dimensional Hamiltonian flows the dynamical zeta function $1/\zeta_j$ has a *double* leading pole coinciding with the leading zero of the F_{j+1} Fredholm determinant.

The effect of such convergence properties of the coefficients on the calculation of classical and quantum escape rates is demonstrated in table 5 and fig. 9.

6 Conclusion

As we have shown in the above, the three-disk system is an ideal model for tests of periodic orbit expansions in hyperbolic systems, not only in the classical but also in the semiclassical context. With a little bit of geometry one can obtain very good estimates for the classical and quantum escape rates as a function of the separation : radius ratio (fig. 3), demonstrating the accuracy of approximating the repeller by a few scales. With numerically obtained periodic orbits up to period 14 one can test the analyticity properties of quantum Selberg zeta functions and

Table 5. Classical and quantum escape rates computed from the Fredholm determinant F_{cl} (11), the quantum Selberg zeta function Z_{qm} (17), and the dynamical zeta function $1/\zeta_0$, as function of the maximal cycle length. Due to the presence of the same pole in both quantum zeta functions, the convergence of the quantum Selberg zeta function is not significantly better than the convergence of the dynamical zeta function. See also fig. 9.

	n	F_{cl}	Z_{qm}	$1/\zeta_0$
	1	0.39	0.11	0.119
	2	0.4105	0.12153	0.12152
	3	0.410338	0.1215574	0.121556
$d : R = 6$	4	0.4103384074	0.121557625	0.12155760
	5	0.4103384077696	0.1215576283	0.121557627
	6	0.410338407769346482	0.1215576284	0.1215576284
	7	0.4103384077693464892	0.1215576284	0.1215576284
	8	0.4103384077693464893 38468	.	.
	9	0.4103384077693464893384613074	.	.
	10	0.410338407769346489 3384613078192	.	.
	1	0.41	-0.076	0.019
	2	0.72	0.041	0.038
	3	0.675	0.04052	0.0403
	4	0.67797	0.040575	0.04054
$d : R = 3$	5	0.677921	0.0405789	0.040575
	6	0.6779227	0.04057935	0.040578
	7	0.6779226894	0.040579405	0.0405793
	8	0.6779226896002	0.0405794102	0.04057940
	9	0.677922689599532	0.0405794108	0.0405794099
	10	0.67792268959953606	0.0405794108	0.0405794107

Fredholm determinants; to our surprise we found that quantum Selberg zeta functions have poles. Their presence spoils the faster than exponential convergence typical of the classical Fredholm determinants; whether their analyticity can be improved is still being investigated. In the case of sufficiently separated three disks, this may not seem to be terribly important (one already has good exponential convergence), but the more poorly converging cycle expansions for spectra of bounded systems also seem to have poles.

Quite generally, despite considerable progress (see, for example, the periodic orbit theory theme issue of *CHAOS* [23]), the semiclassical quantization of bounded systems is still not a routine calculation: all known bounded systems have either pruning, marginally stable periodic orbits and/or accumulating sequences of orbits, and the quantum Selberg zeta functions have poles that degrade the convergence of cycle expansions. We remain optimistic, and believe that in the near future many of these problems will be overcome.
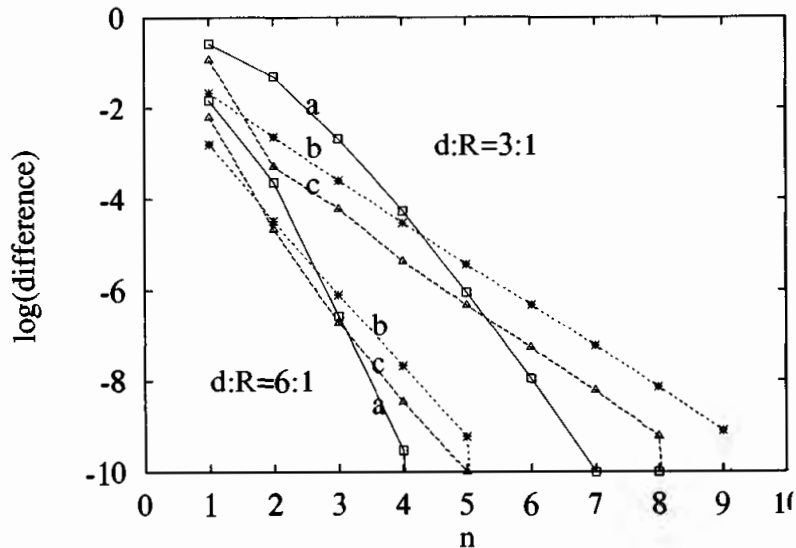
Fig. 9. Convergence of zeros of zeta functions towards the asymptotic values as more and more orbits are included. Shown are the convergence of the classical Fredholm determinant escape rate estimates, the quantum Selberg zeta function lowest resonance estimates, and the quantum $1/\zeta_0$ lowest resonance estimates for ratios $d : R = 6$ and $d : R = 3$. The zero obtained for $n = 14$ has been taken as the asymptotic value. Note the faster than exponential convergence for the classical Fredholm determinant, and the exponential approach for the quantum zeta functions.

Acknowledgements

APPENDIX

A: Numerical determination of periodic orbits

Fixed-point searches based on direct solution of the fixed-point condition (4) as an initial value problem are numerically rather unstable. Methods such as the multipoint shooting or orbit length minimization, described here, are considerably more robust and faster. Other methods for determination of n-disk periodic orbits

are given in refs. [24, 25]. A preliminary step to either calculation is preparation of a list of all distinct allowed prime periodic symbol sequences; an example of such list is given in table 1.

Multipoint shooting method

In the multipoint shooting approach one treats the N cycle points (for example, the five cyclic permutations of $\overline{00101}$) as independent degrees of freedom, and solves the system of equations

$$
\begin{aligned}
T_1 x_{10100} &= x_{01001} \\
T_0 x_{01001} &= x_{10010} \\
T_1 x_{10010} &= x_{00101} \\
T_0 x_{00101} &= x_{01010} \\
T_0 x_{01010} &= x_{10100}
\end{aligned}
\tag{A1}
$$

using the $2N$-dimensional Newton method.

In most of our computations, we fix the ratio $d : R = 6$ and use the fixed points of the maps T_i as starting guesses; the Newton method works quickly and reliably for all the period lengths tested (all orbits of length $N \le 15$). Once a periodic orbit has been found, orbits for different $d : R$ ratios may be obtained by (adiabatically) varying the ratio, and using the old orbit points as starting guesses in the Newton method. This works well for $d : R$ larger than about 2.4. For smaller values, some orbits change rather quickly and require very small step sizes. In addition, for ratios below $d : R = 2.04821419\ldots$ one has to worry about pruning, *i.e.*, the possibility that the minimal length trajectories are blocked by intervening disks. (This problem has no easy solution and is not treated here.)

Orbit length minimization method

The simplest method for determining billard cycles is given by the principle of least action, or, equivalently, by minimizing the length of an approximate orbit that visits a given sequence of disks. In contrast to the multipoint shooting method which requires variation of $2N$ phase-space points, minimization of the cycle length requires variation of only N bounce positions s_i, $i = 1, 2, \ldots, N$.

Let the points (x_i, y_i) denote the centers of the N nonintersecting disks with radii R_i. The length (or equivalently, the period or the action) of the approximate cycle is given by

$$
L = \sum_{i=1}^{N} l_i = \sum_{i=1}^{N} [(\Delta x_i)^2 + (\Delta y_i)^2]^{1/2}
$$

where $\Delta x_i \equiv x_{i+1} - x_i + R_{i+1} \cos(s_{i+1}) - R_i \cos(s_i)$, $x_{N+1} \equiv x_1$, and similarly for

Δy_i. The cycle length varies with variation of s_i as

$$(\vec{\nabla}L)_i = \frac{\partial l_{i-1}}{\partial s_i} + \frac{\partial l_i}{\partial s_i} = R_i \left(\sin(s_i) \left(\frac{\Delta x_i}{l_i} - \frac{\Delta x_{i-1}}{l_{i-1}} \right) - \cos(s_i) \left(\frac{\Delta y_i}{l_i} - \frac{\Delta y_{i-1}}{l_{i-1}} \right) \right) .$$
(A2)

The minimization is achieved by recursive implemention of the following algorithm:

(i) Select an initial set of bounce positions $\vec{s}_0$.

(ii) Evaluate $\vec{\nabla}L \, |_{\vec{s}=\vec{s}_0}$.

(iii) Minimize L along the tangent space spanned by the above gradient, *i.e.*, minimize the function $L(\vec{s}_0 + \vec{\nabla}L \, |_{\vec{s}=\vec{s}_0} \cdot \vec{t})$ with respect to the variation $\vec{t}$.

(iv) Use the bounce points $\vec{s}_1$ so determined as the starting point for the next iteration of the algorithm, until the desired accuracy is attained.

(v) If the dynamics is pruned, check that the final minimal length orbit does not penetrate any of the disks.

The orbit minimization algorithm works very well in practice.

B: Cycle stability for billiards

Consider a two-dimensional billiard with phase space coordinates (q_1, q_2, p_1, p_2). Let t_k be the instant of the k-th collision of the billiard with the billiard boundary, and $t_k^{\pm} = t_k \pm \epsilon$, ϵ positive and infinitesimal. Setting the mass and the velocity equal to 1, we impose energy conservation by parametrizing the momentum direction by angle θ, $(q_1, q_2, \sin\theta, \cos\theta)$. Now parametrize the two-dimensional neighbourhood of a trajectory segment between $(k-1)$-th and k-th collisions by $\delta x = (\delta\theta, \delta z)$, where

$$\delta z_k = \delta q_1 \cos\theta_k - \delta q_2 \sin\theta_k ,$$

is the coordinate variation transverse to the k-th segment of the flow. Using $dq_i/dt = p_i$, we obtain the equations of motion for the linearized neighbourhood

$$\frac{d}{dt}\delta\theta = 0, \quad \frac{d}{dt}\delta z = \delta\theta .$$

Let $\delta\theta_k = \delta\theta(t_k^+)$ and $\delta z_k = \delta z(t_k^+)$ be the local coordinates immediately after the k-th collision, and $\delta\theta_k^- = \delta\theta(t_k^-)$, $\delta z_k^- = \delta z(t_k^-)$ immediately before. Integrating the free flight from t_{k-1}^+ to t_k^- we obtain

$$
\begin{aligned}
\delta\theta_k^- &= \delta\theta_{k-1} \\
\delta z_k^- &= \delta z_{k-1} + \tau_k \delta\theta_{k-1}, \qquad \tau_k = t_k - t_{k-1},
\end{aligned}
$$
(A3)

and the transverse jacobian is given by

$$\mathbf{J}_T(x_k) = \begin{bmatrix} 1 & 0 \\ \tau_k & 1 \end{bmatrix} .$$

At incidence angle ϕ_k (the angle between the outgoing particle and the outgoing

normal to the billiard edge), the incoming transverse variation δz_k^- projects onto an arc on the billiard boundary of length $\delta z_k^- / \cos \phi_k$. The corresponding incidence angle variation $\delta \phi_k = \delta z_k^- / R_k \cos \phi_k$, R_k = the local radius of curvature, increases the angular spread to

$$\delta \theta_k = -\delta \theta_k^- - \frac{2}{R_k \cos \phi_k} \delta z_k^-$$

$$\delta z_k = -\delta z_k^-,$$ (A4)

so the jacobian associated with the reflection is

$$\mathbf{J}_R(x_k) = - \begin{bmatrix} 1 & r_k \\ 0 & 1 \end{bmatrix}, \qquad r_k = \frac{2}{R_k \cos \phi_k}.$$

The jacobian of a cycle p of length n_p is given by

$$\mathbf{J}_p = (-1)^{n_p} \prod_{k=1}^{n_p} \begin{bmatrix} 1 & r_k \\ 0 & 1 \end{bmatrix} \begin{bmatrix} 1 & 0 \\ \tau_k & 1 \end{bmatrix}.$$ (A5)

As $\det \mathbf{J} = 1$, the sign of the leading eigenvalue depends only on the trace of the determinant: $\Lambda = \frac{1}{2}(trJ \pm \sqrt{tr^2 J - 4})$, and by (A5) the trace after n compositions of the determinants has the sign $(-1)^n$, *i.e.*, the eigenvalues flip sign at each collision. This yields a convenient way of finding the correct sign of the stabilities in the fundamental domain, since a straight wall can be considered as the limit of a disk whose radius tends to infinity.

An alternative approach to the eigenvalue evaluation is based on observation that the [2x2] volume preserving matrix multiplication can be achieved by iteration of linear fractional maps;

$$\mathbf{M}_i = \begin{bmatrix} c_i & a_i \\ d_i & b_i \end{bmatrix}, \quad \det \mathbf{M}_i = 1, \quad \rightarrow \quad T_i(z) = \frac{a_i + b_i z}{c_i + d_i z},$$

$$\mathbf{M}_{ij} = \mathbf{M}_j \mathbf{M}_i \quad \rightarrow \quad T_i T_j(z) = \frac{a_i c_j + b_i a_j + (a_i d_j + b_i b_j)z}{c_i c_j + d_i a_j + (c_i d_j + d_i b_j)z}$$

If we represent the translations and the reflections by

$$\mathbf{J}_R(x_k) \quad \rightarrow \quad R_k(z) = r_k + z,$$

$$\mathbf{J}_T(x_k) \quad \rightarrow \quad T_k(z) = \frac{1}{\tau_k + \frac{1}{z}},$$

the k-th segment of the trajectory is represented by

$$T_k R_k(z) = \frac{1}{\tau_k + \dfrac{1}{r_k + z}}.$$ (A6)

For the cycle p the iteration yields

$$z = T_1 R_1 T_2 R_2 \cdots T_{n_p} R_{n_p}(z) = \frac{a_p + b_p z}{c_p + d_p z}.$$ (A7)

For dispersing billiards $r_m > 0$, so all coefficients are positive. The expanding eigenvalue satisfies $|\Lambda_p| + 1/|\Lambda_p| = b_p + c_p$, so the cycle eigenvalue is a root of the quadratic equation

$$|\Lambda_p| = \frac{b_p + c_p + \sqrt{(b_p + c_p)^2 - 4}}{2} = b_p - d_p z_p. \qquad (A8)$$

alternatively given as the root z_p of the linear fractional representation fixed point condition (A7). The sign of Λ_p is $(-1)^{n_p}$.

Eqs. (A3) and (A4) can be rewritten as

$$
\begin{aligned}
\frac{\delta z_k^-}{\delta \theta_k^-} &= \frac{\delta z_{k-1}}{\delta \theta_{k-1}} + \tau_k \\
\frac{\delta \theta_k}{\delta z_k} &= \frac{\delta \theta_k^-}{\delta z_k^-} + \frac{2}{R_k \cos \phi_k},
\end{aligned}
\qquad (A9)
$$

leading to the continued fraction recursion (A6)

$$\kappa_{k-1} = \cfrac{1}{\tau_k + \cfrac{1}{r_k + \kappa_k}}, \qquad \kappa_k = -\frac{\delta \theta_k}{\delta z_k}. \qquad (A10)$$

for the Sinai-Bunimovič curvatures [26, 27]. In other words, the Sinai-Bunimovič continued fraction method of evaluating curvatures (used, for example, in ref. [25]) is identical to multiplying [2x2] jacobian matrices, the method by which we evaluate the stabilities.

Interpretation: imagine a set of projectiles leaving a point (q_1, q_2) in all directions, parametrized by angle θ; they generate a "horocycle" in the configuration space, a set of all points reached by time t. A $\delta\theta$ wedge of angles stretches into a horocycle arc $\delta z = t\delta\theta$, and $\delta\theta/\delta z = 1/t$ is the local curvature of the horocycle [26, 27].

REFERENCES

[1]   M.C. Gutzwiller, *Chaos in Classical and Quantum Mechanics* (Springer, New York 1990)

[2]   A. Selberg, *J. Ind. Math. Soc.* **20**, 47 (1956)

[3]   M.V. Berry and K.E. Mount, *Rep. Prog. Phys.* **35**, 315 (1972)

[4]   D. Wintgen, *Phys. Rev. Lett.* **58**, 1589 (1987)

[5]   B. Eckhardt and E. Aurell, *Europhys. Lett.* **9**, *509 (1989)*

[6]   P. Cvitanović, *Phys. Rev. Lett.* **61**, 2729 (1988)

[7]   R. Artuso, E. Aurell and P. Cvitanović, *Nonlinearity* **3**, 325 (1990)

[8]   P. Cvitanović and B. Eckhardt, *Phys. Rev. Lett.* **63**, 823 (1989)

[9]   D. Ruelle, *Statistical Mechanics, Thermodynamic Formalism* (Addison-Wesley, Reading 1978)

[10] F. Christiansen, G. Paladin and H.H. Rugh, *Phys. Rev. Lett.* **65**, 2087 (1990)

[11] B. Eckhardt, *J. Phys.* A **20**, 5971 (1987)

[12] P. Gaspard and S. Rice, *J. Chem. Phys.* **90**, 2225 (1989)

[13] P. Gaspard and S. Rice, *J. Chem. Phys.* **90**, 2242 (1989); **90**, 2255 (1989)

[14] B. Eckhardt, *Physica* **D 33**, 89 (1988)

[15] P. Cvitanović and B. Eckhardt, *J. Phys.* **A 24**, L237 (1991)

[16] R. Balian and C. Bloch, *Ann. Phys. (NY)* **85**, 514 (1974)

[17] A. Voros, *J. Phys.* **A 21**, 685 (1988)

[18] P.E. Rosenqvist (unpublished)

[19] P. Cvitanović and B. Eckhardt, *Nonlinearity* **6**, 277 (1993)

[20] H.H. Rugh, *Nonlinearity*,**5**, 1237 (1992)

[21] B. Eckhardt and G. Russberg, *Phys. Rev.* **E 47**, 1578 (1993)

[22] P. Cvitanović and P.E. Rosenqvist, *A new determinant for quantum chaos*, Proc. SISSA workshop "From Classical to Quantum Chaos", Trieste (July 1992)

[23] P. Cvitanović, ed., *Periodic Orbit Theory - theme issue*, *CHAOS* **2**, 1-158 (1992)

[24] T. Harayama and A. Shudo, *J. Phys.* **A 25**, 4595 (1992)

[25] P. Gaspard and D. Alonso Ramirez, *Phys. Rev.* **A 45**, 8383 (1992)

[26] Ya.G. Sinai *Usp. Mat. Nauk* **25**, 141 (1970)

[27] L. Bunimovič, *Comm. Math. Phys.* **65**, 295 (1979)